Electrochimica Acta 494 (2024) 144430

Contents lists available at ScienceDirect

Electrochimica Acta

journal homepage: www.journals.elsevier.com/electrochimica-acta

Ultrasensitive and Highly Selective *o*-Phenylenediamine Molecularly Imprinted Polymer for the Detection of 2,4-Dichlorophenoxyacetic Acid

Angelo Tricase [a,b], Verdiana Marchianò [a,b], Eleonora Macchia [a,b,c], Nicoletta Ditaranto [b,d], Luisa Torsi [b,d], Paolo Bollella [b,d,*]

[a] *Department of Pharmacy-Pharmaceutical Science, University of Bari Aldo Moro, Via E. Orabona, 4 – , Bari 70125, Italy*
[b] *Centre for Colloid and Surface Science, University of Bari Aldo Moro, Via E. Orabona, 4 –, Bari 70125, Italy*
[c] *Faculty of Science and Engineering, Åbo Akademi University, Turku 20500, Finland*
[d] *Department of Chemistry, University of Bari Aldo Moro, Via E. Orabona, 4 –, Bari 70125, Italy*

ARTICLE INFO

Keywords:
2,4-dichlorofenoxyacetic acid
Modified electrodes
Molecularly imprinted polymers (MIPs)
o-phenylenediamine
Template removal

ABSTRACT

Herein, we report an ultrasensitive and highly selective analytical methods to detect 2,4-dichlorophenoxyacetic acid (2,4-D) using an *o*-phenylenediamine based molecularly imprinted polymer (*o*-PD-MIP) sensor. Electrochemical Quartz Crystal Microbalance (EQCM) is used to investigate both the kinetics and the mass of the electropolymerized *o*-phenylenediamine. Additionally, successful removal of the template from the imprinted cavities is confirmed by comparing the XP spectra of imprinted and o-PD-MIPs after various template removal procedures. The most effective method involves a 70:30 mixture of MeOH:H_2O for 15 min under stirring. The *o*-PD-MIP sensor exhibits high sensitivity with a LoD of $(3 \pm 1) \times 10^{-12}$ M, which is below the EU regulation limits for drinking water by six orders of magnitude, a linear range between 10 and 100pM, and an excellent selectivity. These results proved the effectiveness of template removal procedure by using a 70:30 MeOH:H_2O mixture and are a proof-of-concept for ultrasensitive and selective 2,4-D detection in real samples.

1. Introduction

The widespread deployment of herbicides, insecticides, and fungicides in agricultural settings has increased the contamination of pivotal environmental reservoirs (*e.g.,* soil matrices, groundwater reservoirs, and surface water bodies) [1–3]. Despite their role in increasing agricultural productivity and preserving crop integrity, these chemical agents frequently cause risks to both biotic and abiotic components of ecosystems [4]. Among these chemical agents, 2,4-dichlorophenoxyacetic acid (2,4-D) stands out as a widely utilized herbicidal agent renowned for its efficacy in eradicating broadleaf weed species across diverse agricultural, silvicultural, and infrastructure management contexts [5,6]. Despite its effectiveness in weed control, 2,4-D has been associated with numerous adverse health effects. Studies have linked its exposure to carcinogenic activity, implicating it in the development of cancer in humans [7]. Furthermore, 2,4-D has been identified as an endocrine disruptor, capable of interfering with hormonal balance and reproductive functions. Acute exposure to this herbicide has also been shown to induce congestion and degenerative changes in the central nervous system, raising concerns about its neurotoxic effects [8,9].

Given the potential risks associated with 2,4-D and other pesticide residues, regulatory bodies such as the European Drinking Water Act (EDWA) have established stringent guidelines to limit their presence in drinking water [10]. These regulations set maximum allowable concentrations for individual pesticides and the combined total of pesticides, underscoring the importance of monitoring, and controlling these contaminants to ensure the safety of drinking water supplies [11]. Hence, there is a pressing need for robust monitoring systems and analytical techniques capable of detecting and quantifying pesticide residues, including 2,4-D, in various environmental matrices [12]. Such monitoring efforts are essential for identifying potential sources of contamination, assessing the extent of environmental pollution, and implementing targeted remediation strategies to mitigate the adverse effects of pesticide exposure on both human health and the environment [13,14]. Currently, common methods for analyzing 2,4-D involve techniques like high-performance liquid chromatography (HPLC) [15], liquid chromatography–mass spectrometry (LC–MS) [16], gas chromatography (GC) [17], and capillary electrophoresis (CE) [18]. However,

* Corresponding author at: Department of Chemistry, University of Bari Aldo Moro, Via E. Orabona, 4 –, Bari 70125, Italy.
E-mail address: paolo.bollella@uniba.it (P. Bollella).

https://doi.org/10.1016/j.electacta.2024.144430
Received 13 February 2024; Received in revised form 25 April 2024; Accepted 12 May 2024
Available online 13 May 2024

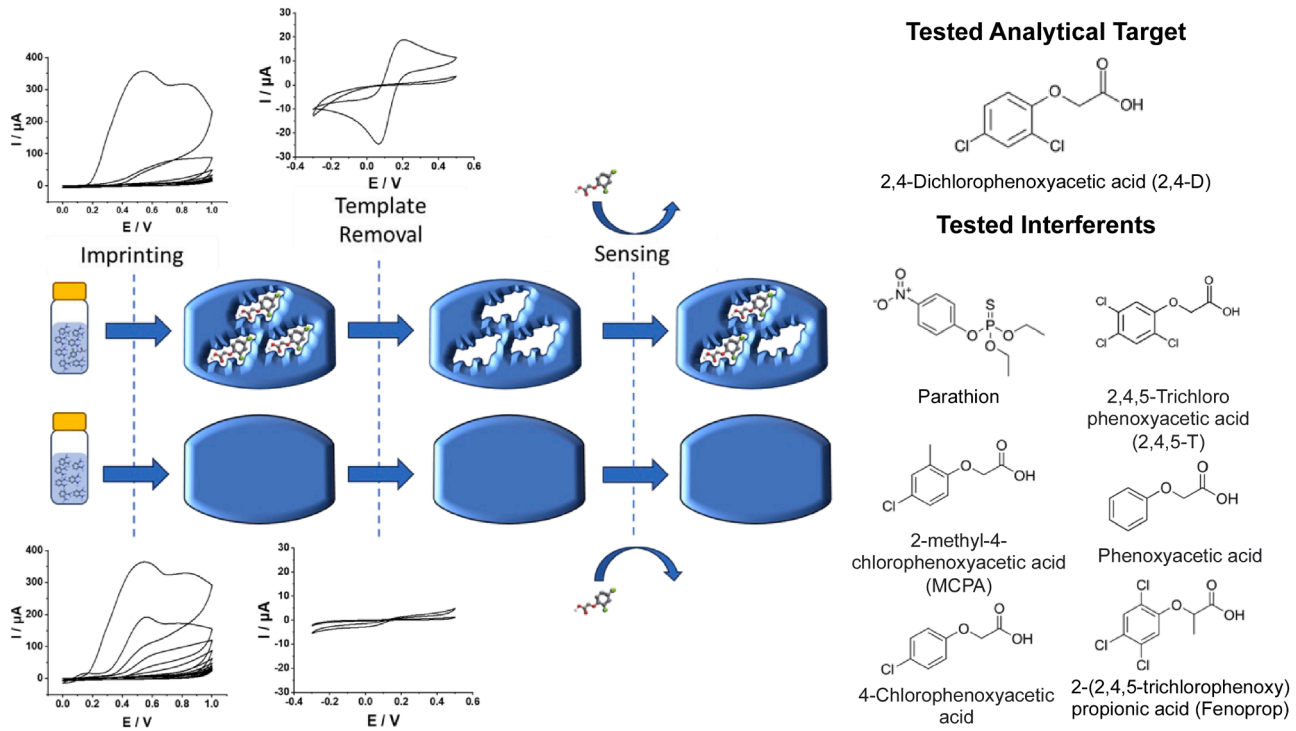

Fig. 1. Schematic workflow for MIP (top) and NIP (bottom) electropolymerization. Cyclic voltammograms of the electropolymerization (imprinting) were reported above (MIP) and below (NIP) the first step. Cyclic voltammograms in 5 mM $Fe(CN)_6^{3-/4-}$ solution before and after the template removal step were reported above (MIP) and below (NIP) the second step. Chemical structures of tested analytical target and interferents with MIP and NIP.

these methods require expensive equipment, complex sample preparation, and skilled personnel, making on-site detection challenging. Additionally, certain antibody-based immunosensors have been developed for 2,4-D detection based on colorimetric responses. Nevertheless, they suffer from drawbacks such as instability of antibodies or enzymes, restricting their utility in detecting real samples [19–23].

On the other hand, molecular and biomolecular recognition techniques find widespread application in the development of sensing devices for detecting contaminants in biological, food, and environmental samples. Bio-inspired recognition elements are pivotal in enhancing the sensitivity of biosensors [24–26]. These elements mimic affinity interactions such as antibody-antigen or antibody-antibody interactions, and hybridization reactions like aptamer mismatch, through the synthesis of artificial bio-inspired receptors [27]. Molecularly imprinted polymers (MIPs) are considered the closest synthetic analogs to antibody-antigen systems, operating on a lock-and-key mechanism to selectively bind target molecules [28,29]. MIPs are utilized across various fields including sample preparation, chromatography, chemical sensing, and drug delivery [30,31]. They offer similar selectivity and sensitivity to bioreceptors but are more cost-effective and easily customizable for a wide range of analytical targets. MIPs are typically prepared using conducting polymers like polypyrrole or poly(*o*-phenylenediamine) via chemical or electrochemical polymerization methods [32–35]. Despite their utility, MIPs face challenges during washing steps, with issues such as incomplete template removal and a lack of clarity regarding the removal mechanism [36]. Interactions utilized in MIP development, such as electrostatic Van der Waals interactions and hydrogen bonding, are relatively weak [37]. While many studies discuss MIP preparation, effectiveness, and cost, the efficiency of template removal is often overlooked [38]. Template removal methods commonly involve incubation in organic solvents or salt solutions, but complete removal is hindered by factors like poor solvent diffusion, highly cross-linked regions, or low template solubility. Schweiger et al. recently proposed a template removal procedure based on pulsed amperometric detection (PAD), coupled with X-ray photoelectron spectroscopy (XPS) analysis, which demonstrated complete removal of the template. XPS analysis is frequently used to assess the efficacy of washing treatments and examine structural modifications in MIPs post-washing, which may impact their rebinding properties [39,40].

Herein, we report on the electropolymerization of *o*-PD in the presence and absence of 2,4-D, as templating analytical target, to obtain MIPs and NIPs, respectively (Fig. 1). The proposed MIPs and NIPs were characterized by electrochemical quartz crystal microbalance (EQCM) to investigate both the kinetics and the polymeric mass deposited onto the electrode surface. Moreover, several template removal protocols, including strong acid/base solutions and aqueous/organic solutions, were investigated both with MIPs and NIPs to ensure a complete template removal by XPS analysis. The *o*-PD-MIP sensor was able to detect 2,4-D in the range 3–100 pM by using square wave voltammetry (SWV) in $Fe(CN)_6^{3-/4-}$ as redox probe. Structurally similar molecules (e.g., 2,4,5-trichlorophenoxyacetic acid (2,4,5-T), 2-methyl-4-chlorophenoxyacetic acid (MCPA)), phenoxyacetic acid (PA, aromatic ring without chloride), 4-chlorophenoxyacetic acid (4-CPA, aromatic ring with one chloride atom) and 2-(2,4,5-trichlorophenoxy)propionic acid (2-(2,4,5-T)PA, longer lateral chain) and other pesticides like parathion were tested as potential interfering compounds (range 1 - 1 × 10^6 pM), proving the extremely high selectivity of the proposed platform for 2,4-D detection.

2. Experimental

2.1. Materials and reagents

4-(2-hydroxyethyl)piperazine-1-ethanesulfonic acid (HEPES), acetonitrile (ACN), methanol (MeOH), potassium chloride (KCl), potassium ferrocyanide ($K_4[Fe(CN)_6]$), potassium ferricyanide ($K_3[Fe(CN)_6]$), sodium acetate (CH_3COONa), *o*-phenylenediamine (*o*-PD), 2,4-dichlorophenoxyacetic acid (2,4-D), parathion, HPLC grade H_2O, 2,4,5-trichlorophenoxyacetic acid (2,4,5-T), 2-methyl-4-chlorophenoxyacetic acid (MCPA), phenoxyacetic acid (PA), 4-chlorophenoxyacetic acid (4-

CPA) and 2-(2,4,5-trichlorophenoxy)propionic acid ((2-(2,4,5-T)PA) were purchased by Merck Millipore (formerly Sigma Aldrich) and used without further purification.

HEPES buffer was prepared dissolving HEPES and KCl in water (10 mM HEPES, 100 mM KCl) and adjusting the pH to 7.2 using NaOH 1 M. $Fe(CN)_6^{3-/4-}$ solution was prepared dissolving $K_3[Fe(CN)_6]$ and $K_4[Fe(CN)_6]$ in HEPES buffer (5 mM $K_4Fe(CN)_6$, 5 mM $K_3Fe(CN)_6$). This solution was diluted in HEPES buffer to a ratio of 1:1 before the electrochemical measurement (5 mM as total concentration of redox probe). Acetate buffer was prepared dissolving sodium acetate in water (100 mM) and adjusting the pH to 5.8 using HCl 1 M. *o*-PD solution was dissolved in acetate buffer (7.5 mM) and used without further modification for NIP electropolymerization. 2,4-D was first solubilized in methanol (100 mM) and diluted 1:100 using *o*-PD solution for MIP electropolymerization. 2,4-D and parathion solution for sensing experiments were prepared progressively diluting 1:10 the stock solution (100 mM in methanol) in Milli-Q water. All solutions for electrochemical measurements were prepared using Milli-Q water (18.2 MΩ cm, Millipore, Bedford, MA, USA).

2.2. Electrochemical setup

All electrochemical measurements were conducted using a PalmSens4 potentiostat equipped with PSTrace 5.6v software (except for EQCM). Commercially available screen-printed gold electrodes (DRP-220BT, named Au-SPE), comprising a circular gold working electrode (with a geometric area of 12.6 mm^2), a gold counter electrode, and a silver pseudo-reference electrode, were purchased by Metrohm and utilized for all the electrochemical measurements (except for E-QCM). All potential values reported in the manuscript are expressed vs. Ag pseudo-reference electrode.

2.3. MIP and NIP electropolymerization, template removal and rebinding

Au-SPE electrodes were polished via electrochemical cleaning using cyclic voltammetry in 0.5 M H_2SO_4 solution within a potential range of 0–1.4 V for 25 cycles at a scan rate of 0.3 V s^{-1}. Afterwards, *o*-PD were electropolymerized on the electrodes through consecutive cyclic voltammetry in MIP and NIP solutions for 10 cycles at a scan rate of 0.2 V s^{-1} within a potential range of 0.0 V to 1.0 V. The MIP and NIP-modified Au-SPEs were treated with various washing solutions to remove the template, including EtOH:HCl:KCl (pH 2.5), NaOH 0.1 M (pH 13), ACN:H_2O mixtures of varying ratios (10:90, 30:70, 50:50), and MeOH:H_2O mixtures (50:50, 70:30) [37]. Template removal was confirmed using cyclic voltammetry (CV) and X-ray photoelectron spectroscopy (XPS). Afterwards, *o*-PD electropolymerization was optimized according to the approach one-variable-at-time (OVAT) investigating the number of cycles (2, 4, 8, 10, 15, 20), scan rate (0.02 V s^{-1}, 0.05 V s^{-1}, 0.1 V s^{-1}, 0.2 V s^{-1}, 0.3 V s^{-1}), and monomer/analytical target ratio (1, 2.5, 5, 7.5, 10). The electrodes performance was evaluated in terms of recovery factor (%) after template removal.

The washed MIP and NIP-modified Au-SPEs were exposed to increasing concentrations (from 0 pM to 1 μM) of 2,4-dichlorophenoxyacetic acid (2,4-D), used as analytical target, parathion, 2,4,5-trichlorophenossyacetic acid (2,4,5-T), and 2-methyl-4-chlorophenoxyacetic acid (MCPA), phenoxyacetic acid, 4-chlorophenoxyacetic acid and 2-(2,4,5-trichorophenoxy)propionic acid (fenoprop) used as negative controls. Additionally, NIP-modified Au-SPEs were investigated with both the analytical target and all interferents. For each concentration, the electrodes were exposed to 60 μL of solution for 15 min, followed by square wave voltammetry (SWV) with the following parameters: E_0= −0.2 V, E_i= 0.5 V, amplitude of 0.05 V, and frequency of 5 Hz. All measurements were performed for n = 3 electrodes, each measured 3 times to increase S/N ratio. The analysis on real samples was performed by spiking with 50 pM 2,4-dichlorophenoxyacetic acid soil (extracted with pure methanol), river water and tap water samples. For each sample, the electrodes were exposed to 60 μL of solution for 15 min, followed by square wave voltammetry (SWV) with the following parameters: E_0= −0.2 V, E_i= 0.5 V, amplitude of 0.05 V, and frequency of 5 Hz. All measurements were performed for n = 3 electrodes, each measured 3 times to increase S/N ratio.

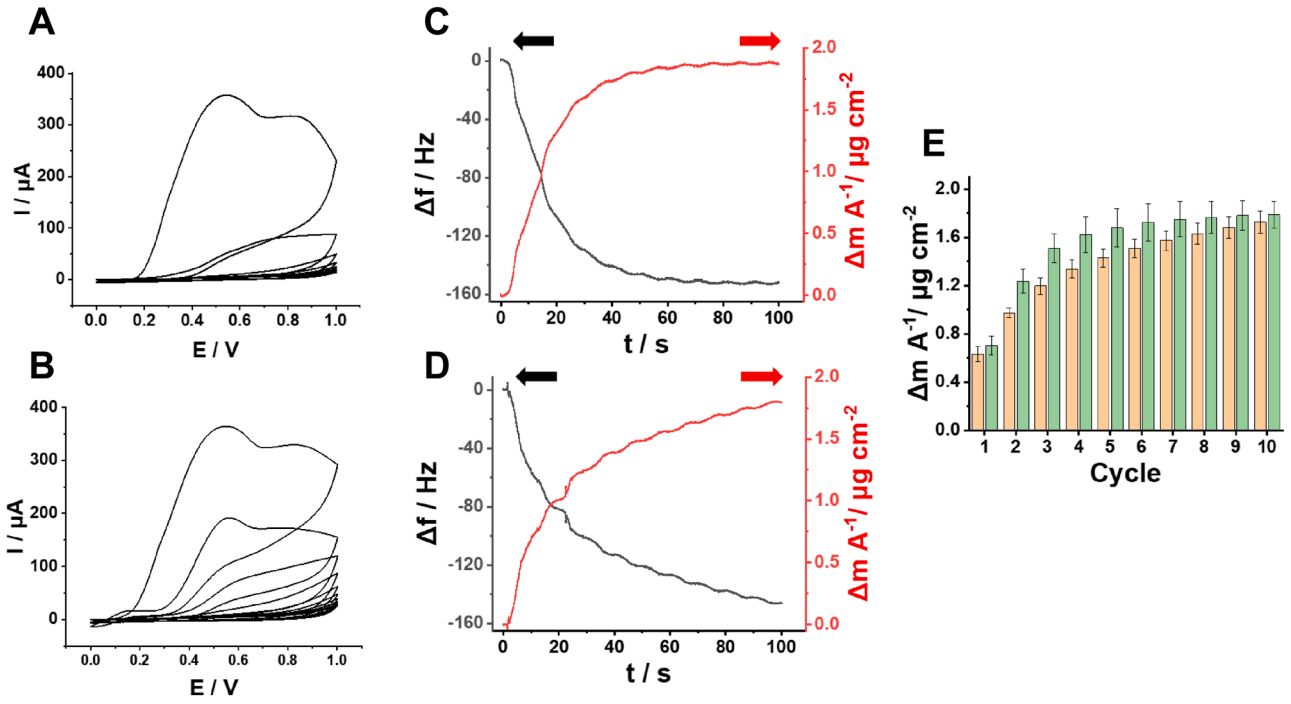

Fig. 2. **(A)** o-PD-MIP electropolymerization, **(B)** o-PD-NIP electropolymerization, **(C)** QCM frequency (black) and relative mass (red) changes during the o-PD-MIP electropolymerization, **(D)** QCM frequency (black) and relative mass (red) changes during the o-PD-NIP electropolymerization, **(E)** relative mass increasing at the end of each polymerization cycle for o-PD-MIP (green) and o-PD-NIP (orange). Error bars described the relative standard deviation (n = 3).

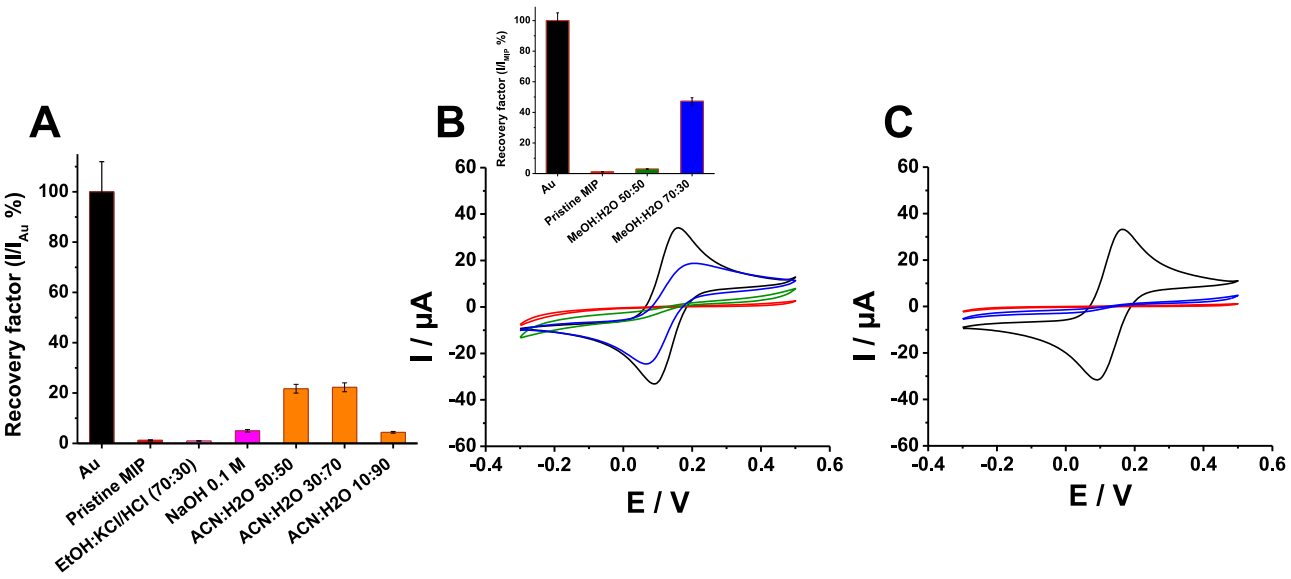

Fig. 3. Template removal protocol evaluation, performed by CVs in 5 mM $Fe(CN)_6^{3-/4-}$ (scan rate 0.01 V s^{-1}). The recovery factor was reported as the percentual ratio between current value recorded at 0.16 V for modified electrodes and for gold. (**A**) recovery factor for gold electrode, pristine o-PD-MIP and o-PD-MIP washed with ethanol:KCl:HCl solution (pH 2.5), NaOH 0.1 M (pH=13), ACN:H_2O 50:50, ACN:H_2O 30:70 and ACN:H_2O 10:90. **B)** CVs recorded on gold (black), pristine o-PD-MIP (red) and o-PD-MIP washed with MeOH:H_2O 50:50 (green) and MeOH:H_2O 70:30 (blue). In the inset the recovery factor for each electrode. (**C)** CVs recorded on gold (black), pristine NIP (red) and NIP washed with MeOH:H_2O 70:30 (blue).

2.4. Electrochemical quartz crystal microbalance

Electrochemical Quartz Crystal Microbalance (EQCM) measurements were conducted using a Metrohm EQCM module installed in an AUTOLAB potentiostat (PGSTAT302N). The module was connected to an EQCM oscillator via a 9-pin sub-D connector. A 6 MHz Au/TiO_2 crystal served as the working electrode, with an Ag/AgCl (3 M KCl) electrode as reference, and a gold coil as counter electrode. EQCM measurements were used to investigate MIP and NIP electropolymerization, by measuring the variation of quartz crystal oscillation frequency. The frequency variation was used to calculate mass variation using Sauerbrey equation:

$$\frac{\Delta m}{A} = -\frac{\Delta f * \sqrt{\rho_q \mu_q}}{f_0^2}$$

where Δm is the mass change, A is the piezoelectrically active crystal Area, Δf is the frequency change, ρ_q is the density of quartz (2.648 g cm^{-3}), μ_q is the shear module of a quartz for AT-cut crystal (2.947×10^{11} g cm^{-1} s^{-2}), and f_0 is the resonant frequency of the fundamental mode (6 MHz). All data were analyzed using Nova 2.1.7 and Origin2021. Mass change per area was reported as Δm/A.

2.5. X-ray photoelectron spectroscopy

X-ray Photoelectron Spectroscopy (XPS) analyses were conducted utilizing a Versa Probe II Scanning XPS Microprobe spectrometer manufactured by Physical Electronics GmbH in Feldkirchen, Germany. The measurements utilized a monochromatized AlKα source with a 200 µm x-ray spot, operating at a power of 104.1 W. Wide scans and detailed spectra were obtained in constant analyzer energy (CAE) mode, employing pass energies of 117.40 eV and 29.35 eV, respectively. Charge compensation was achieved using an electron gun set to 1.0 V and 20.0 µA. All binding energies were calibrated with respect to the C-C component of C1s at 284.8 ± 0.1 eV for adventitious carbon, cross-verified with the Au4$f_{7/2}$ component at 84.0 ± 0.1 eV. Data processing was carried out using MultiPak software version 9.9.0.8 released in 2018 (ULVAC-PHI, Inc., Hagisono, Chigasaki, Kanagawa, Japan) [41].

3. Results and discussion

o-PD electropolymerization for MIP deposition was optimized by considering three parameters (one-variable-at-time, OVAT approach): number of scans, scan rate and monomer/tamplate ratio. The electrodes performance was evaluated in terms of recovery factor (%) after template removal (**Fig. SI1**, supporting information). *o*-PD-MIP electrodes reported the highest recovery at 10 scans, 0.2 V s^{-1} as scan rate and monomer/template ratio of 7.5. These parameters were employed to further characterize *o*-PD-MIP and *o*-PD-NIP and evaluate their analytical performance. To evaluate the electrochemical and piezoelectrical features of *o*-PD-MIP and *o*-PD-NIP, both electropolymerized platforms were characterized by CVs in $Fe(CN)_6^{3-/4-}$ and performing the EQCM experiments during the electrochemical polymerization. Both *o*-PD-MIP and *o*-PD-NIP electropolymerizations were performed as described in Section 2.3. Fig. 2A **and** B report the CVs for the electropolymerization of *o*-PD-MIP and *o*-PD-NIP, respectively. Both CVs sequences showed a constant current decreasing from the first to last cycle, which can be ascribed to *o*-PD film growth onto the gold surface. The *o*-PD film, in both cases, was self-limiting the uncontrolled growth of the polymer. In both *o*-PD-MIP and *o*-PD-NIP, the first half-cycle resulted similar, showing two main peaks centered around +0.5 and +0.7 V, respectively, and related to *o*-phenylendiamine oxidation and overoxidation. This is a common pathway for *o*-phenylendiamine electropolymerization carried out at pH 5 or higher, as reported in the literature [42]. Based on the current trend from the second CV, *o*-PD-MIP showed a remarkably faster kinetics than *o*-PD-NIP during the electropolymerzation, mainly due to electrostatic interactions triggering a faster growth in presence of templating molecule. Indeed, *o*-PD polymerization is typically related to the formation of a positively charged oxidated intermediate [42], while the 2,4-D is mainly negatively charged at pH 5.8 (pKa = 2.85) [43]. Hence, the deprotonated 2,4-D triggers the reaction between positively charged overoxidized monomers, accelerating the polymerization rate.

Fig. 2C **and** D report the crystal frequency (black curve) and mass (red curve) changes for NIP and MIP. The crystal frequency was recorded during the electropolymerization, while mass change was calculated by using Sauerbray equation [44]. Frequency and mass trends are equal but opposite in sign, so the decrease in frequency during the experiment

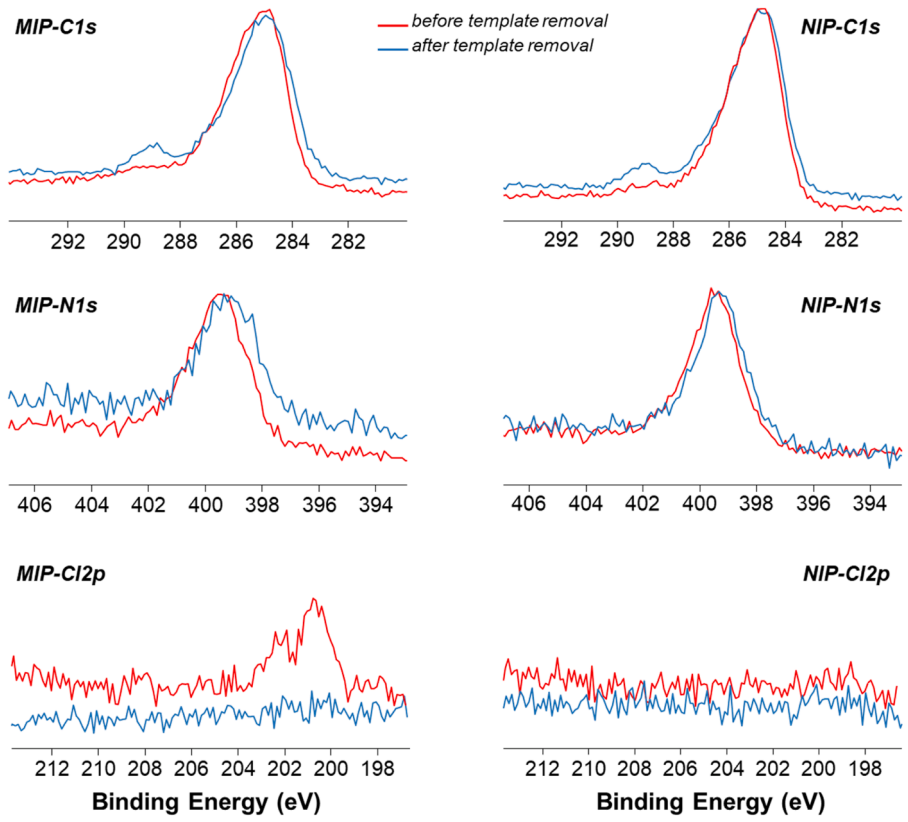

Fig. 4. C1s, O1s, and Cl2p XP spectra for o-PD-MIPs (left panel) and o-PD-NIPs (right panel) before (red) and after (blue) template removal with 70:30 MeOH: H_2O mixture.

corresponded to an increase in mass, confirming the polymer growth during the process. The increase in mass showed a waving trend, characterized by periodic increase/decrease in mass rate growth, which corresponded to the oxidation/reduction half-cycles, respectively. Indeed, the oxidation half-cycles correspond to the formation of positively charged *o*-PD radicals, which are involved in the propagation of chain reaction. The kinetics for *o*-PD-MIP and *o*-PD-NIP growth resulted different, confirming the trends recorded by CV. Indeed, the final mass growth was similar (~1.7–1.8 μg cm^{-2}). Notably, *o*-PD-MIP mass reached a steady-state after 4–5 cycles while *o*-PD-NIP mass continuously increased through all the cycles. This difference confirmed the template role in accelerating the kinetics of polymerization reaction. Fig. 2E reports the histograms of relative mass change for *o*-PD-MIP and *o*-PD-NIP, green and orange bars, respectively. The total relative mass variations for *o*-PD-MIP and *o*-PD-NIP were 1.8 ± 0.1 and 1.7 ± 0.1 μg cm^{-2}, respectively. Prior their use for biosensing, *o*-PD-MIP-modified electrodes were tested towards different template removal protocols to obtain the cavities available for analytical target rebinding. Moreover, template removal protocols using extreme conditions (e.g., concentrated acid/base solutions or undiluted organic solvents) can modify the polymer morphology [37]. Indeed, different combinations of acid, alkaline, and organic solution were tested on both *o*-PD-MIP and *o*-PD-NIP modified electrodes, to analyze both the template removal and poly-o-PD film stability. Bare gold electrodes, pristine *o*-PD-MIPs and washed *o*-PD-MIPs were tested by CV in $Fe(CN)_6^{3-/4-}$ solution (5 mM total concentration in HEPES 10 mM, KCl 0.1 M) to investigate the recovery factor for each template removal protocol (Fig. 3).

CVs recorded on bare gold showed two main peaks due to oxidation/reduction of $Fe(CN)_6^{3-/4-}$while pristine *o*-PD-MIP-modified electrodes showed no peaks, due to the presence of a layer hindering the diffusion of the redox probe towards the electrode surface (Fig. 3B, black and red curves). An effective template removal protocol can quantitatively remove the templating molecule, showing a couple of redox peaks with lower intensity than pristine *o*-PD-MIP-modified electrodes. As quantitative parameter was chosen the current peak (I_{pa}) for the anodic reaction (the peak at +0.16 V for the bare gold electrode was used as reference value). The template removal usually occurs by breaking the hydrogen bonding network between polymer and template through the protonation/deprotonation of the carboxylic/amidic functional groups in the structure. [45] For instance, acidic (EtOH:HCl:KCl, pH 2.5) and alkaline (NaOH 0.1 M, pH 13) template removal protocols were used, obtaining very low recovery factors for both protocols (lower than 10 % in both cases, Fig. 3A). For this reason, a different protocol was selected, varying solution polarity by mixing water and organic solvents. ACN: H_2O protocol showed a higher template removal, with a low recovery factor for 10:90 solution but ~20 % for 30:70 and 50:50 concentrations (Fig. 3A). However, the same protocols, applied to *o*-PD-NIP modified electrodes, showed similar results because of the unselective removal of polymerized *o*-PD from the electrode surface (*data not shown*). Afterwards, MeOH:H_2O mixture was tested reporting a low recovery factor for 50:50 MeOH:H_2O mixture while a recovery factor higher than 50 % (Fig. 3B) and no effect on *o*-PD-NIP modified electrodes (Fig. 3C) by using 70:30 MeOH:H_2O mixture. To confirm the electrochemical results *o*-PD-MIPs and *o*-PD-NIPs, before and after template removal procedure, were investigated using x-ray Photoelectron Spectroscopy (XPS). In particular, C1s and N1s spectral regions were curve-fitted (**Figure SI2**) to confirm poly-*o*-PD structure with and without the analytical target. In both cases C1s and N1s showed peaks ascribable to the poly-*o*-PD structure: BE=284.8 ± 0.1 eV (C-H, C-C), BE=286.2 ± 0.1 eV (C-OH, C-N, C-N^+), BE=287.6 ± 0.1 eV (C=O, C=N), BE=289.3 ± 0.1 eV (C-OOH), BE=398.5 ± 0.2 eV (N=C), BE=399.5 ± 0.2 eV (N-H), BE=400.8 ± 0.3 eV (N^+-C) [46,47]. The presence of 2,4-D just resulted in a slight higher relative abundance of carboxylic component in carbon signal of *o*-PD-MIPs.

Furthermore, C1s, N1s, and Cl2p line-shape of *o*-PD-MIPs and *o*-PD-NIPs, before and after template removal, were compared (Fig. 4).

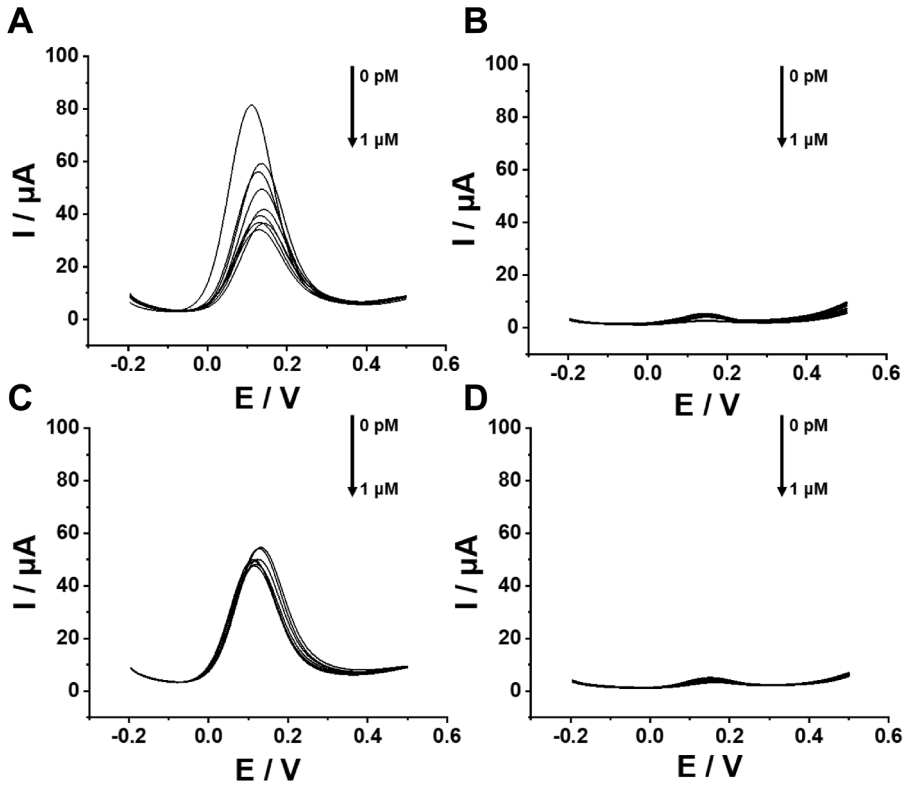

Fig. 5. SWVs in $Fe(CN)_6^{3-/4-}$ (E_0= −0.2 V, E_i= 0.5 V, amplitude 0.05 V, frequency of 5 Hz) for **A)** o-PD-MIP exposed to 2,4-D, **B)** o-PD-NIP exposed to 2,4-D, **C)** o-PD-MIP exposed to parathion, **D)** o-PD-NIP exposed to parathion. Each concentration was tested by casting 60 µL of analyte solution for 15 min, then the sample was washed with Milli-Q H_2O and analyzed. Concentration range: 0pM (HPLC grade H_2O, used as baseline), 1–10–100pM, 1–10–100 nM, 1 µM.

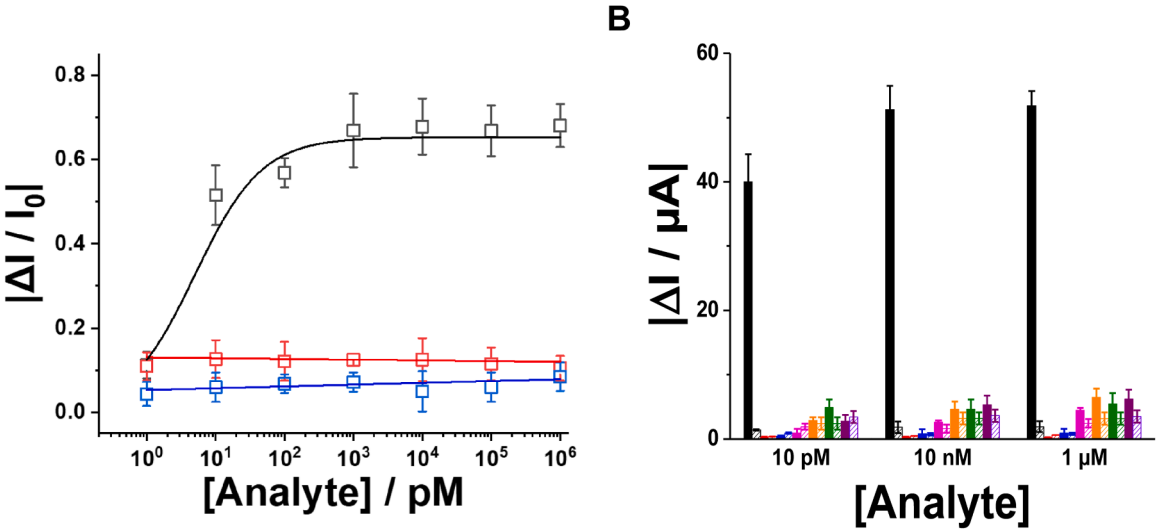

Fig. 6. (. A) Calibration curve for o-PD-MIP exposed to 2,4-D (black points), for o-PD-MIP exposed to parathion (red points), and for -PD-NIP exposed to 2,4-D (blue points). Lines corresponded to the fitting obtained by each data set, using the same color code. **(B)** Current response at 10pM, 10 nM and 1 µM reported as ΔI for o-PD-MIP exposed to 2,4-D (black bars),parathion (red bars), 2,4,5-T (blu bars), MCPA (magenta bars), phenoxyacetic acid (orange bars), 4-chlorophenoxyacetic acid (green bars) and 2-(2,4,5-trichlorophenoxy)propionic acid (purple bars); o-PD-NIP exposed to 2,4-D (black patterned bars), parathion (red patterned bars), 2,4,5-T (blu patterned bars), MCPA (magenta patterned bars), phenoxyacetic acid (orange patterned bars), 4-chlorophenoxyacetic acid (green patterned bars) and 2-(2,4,5-trichlorophenoxy)propionic acid (purple patterned bars); $n = 3$.

Noteworthy, Cl2p spectral region showed the disappearance of Cl-Aryl peak at ~200 eV after template removal. No remarkable changes were detected in carbon and nitrogen signals after template removal for both the samples, but a small increase of the carboxylic component. Since it was found also on *o*-PD-NIP, it was ascribed to a negligible carbon oxidation, probably due to the template removal procedure, rather than arising from traces of 2,4-D. Rather, chlorine is a specific marker for the template (no Cl atoms in PD monomers) and so Cl2p spectra unequivocally proved the efficient template removal.

After template removal *o*-PD-MIPs and *o*-PD-NIPs were exposed to HPLC grade H_2O, used as blank, and to different concentrations of 2,4-D (from 1pM to 1 µM) to test the amperometric response towards different

Table 1
Recovery on soil, river and tap water samples spiked with 50 nM of 2,4-D analyzed by using o-PD-MIP electrodes. Incubation: HPLC grade solutions; Measurements: in $Fe(CN)_6^{3-/4-}$ (E_0= −0.2 V, E_i= 0.5 V, amplitude 0.05 V, frequency of 5 Hz).

Real samples	Found value / nM	Nominal value / nM	Recovery
Soil	47.2 ± 3.4	50	94.4%
River water	51.3 ± 3.1	50	102.6%
Tap Water	45.8 ± 4.2	50	91.6%

Table 2
Comparison between references [21,48–53] and this work. First column: molecules used for MIP growing (template, monomer etc.). Second column: Transducer. Third column: Limit of Detection (LOD) reported in pM with standard deviation (for data reported with ° the standard deviation was not available).

MIP	Transducer	LOD (pM)	Linear range (pM)	Ref.
2,4-D (template) methacryilic acid (monomer) ethylene glycol dimethacrlylato (crosslinker) 2,2′-azobisisobutyronitrile (initiator)	MIP-NPs-SPE	5.0 ± 0.2 * 10^3	2 × 10^4–3 × 10^6	[48]
2,4-D (template) *N*-methacryloyl-(l)-tryptophan methyl ester (monomer) ethylene glycol dimethacrylate (crosslinker) azobisisobutyronitrile (initiator)	QCM and SPR	4.36 ± 0.04 * 10^2	2 × 10^3–8 × 10^4	[21]
2,4-D/TBAH (template) *N*-allyl-4-amino-substituted 1,8-naphthalimide (monomer) Thiourea (fluorophore)	Optic	5 * 10^4 °	2 × 10^5–8 × 10^9	[49]
2,4-D (template) pyrrole (monomer) CTAB (stabilizer)	Amperometric	1 * 10^6 °	n.a.	[50]
2,4-D (template) pyrrole (monomer)	Potentiometric	1 * 10^2 °	3 × 10^2–6 × 10^3	[51]
2,4-D (template) 2- hydroxyethyl methacrylate (monomer) Itaconic acid (IA) ethylene glycol dimethacrylate (crosslinker)	Potentiometric	1 * 10^4 °	n.a.	[52]
2,4-D (template) 4-vinyl pyridine (monomer) ethylene glycol dimethacrylate (crosslinker)	Amperometric	4 * 10^3 °	2 × 10^5–1 × 10^8	[53]
2,4-D (template) *o*-phenylenediamine (monomer)	Amperometric	3 ± 1	10–100	This work

target concentrations (Fig. 5**A and B**). Additionally, *o*-PD-MIPs and *o*-PD-NIPs were characterized by scanning electron microscopy to prove the morphological variation occurring during template removal and incubation with HPLC grade water used to record the baseline of *o*-PD-MIP sensor for 2,4-D detection (**Figure SI3**). *o*-PD-MIPs did not show any variation after template removal. However, *o*-PD-MIP swelling was observed after incubation with HPLC grade water due to morphological modification and decreasing of cavities number available for target rebinding. *o*-PD-NIPs did not show any variation.

The peak current value constantly decreased from 80 μA to 35 μA for *o*-PD-MIP modified electrodes, due to the rebinding of increasing 2,4-D concentrations (Fig. 5A). *o*-PD-NIP modified electrodes did not show any peak current decreasing due to the absence of imprinted cavities able to selectively rebind the analytical target (Fig. 5B). To test the selectivity of the platform, the same experiments were performed on both *o*-PD-MIP and *o*-PD-NIP modified electrodes using parathion in the same concentration range (Fig. 5C **and** D), which is a potential interferent in drinking water sample. No peak current decreasing was observed for *o*-PD-MIP in the presence of parathion, proving its high selectivity in a wide concentration range (1 −1 × 10^6 pM). Fig. 6A shows the normalized relative peak current variation ($\Delta I/I_0$) versus analyte concentration (logarithmic scale, *o*-PD-MIP with 2,4-D, black curve, *o*-PD-MIP with parathion, red curve, and *o*-PD-NIP with 2,4-D, blue curve). *o*-PD-MIP modified electrodes showed a limit of detection (LoD) of 3 ± 1pM (calculated as $\overline{x_b} + 3\sigma_b$ where $\overline{x_b}$ is the averaged blank signal and σ_b is the standard deviation of averaged blank signal $n = 3$). Moreover, *o*-PD-MIP modified electrodes reported a linear range 10–100pM.

o-PD-MIP was also tested against two structural interferences, 2,4,5-trichlorophenoxyacetic acid (2,4,5-T, one chloride atom more than 2,4-D) and 2-methyl-4-chlorophenoxyacetic acid (MCPA, one chloride atom replaced by a methyl group), phenoxyacetic acid (PA, aromatic ring without chloride), 4-chlorophenoxyacetic acid (4-CPA, aromatic ring with one chloride atom) and 2-(2,4,5-trichlorophenoxy)propionic acid (2-(2,4,5-T)PA, longer lateral chain) as reported in Fig. 6B. 2,4,5-T, MCPA, PA, 4-CPA and 2-(2,4,5-T)PA showed an interference of 5 % in the picomolar range and less than 10–15 % in the nanomolar and micromolar range, proving an extremely high selectivity for the proposed *o*-PD-MIP modified electrodes. Particularly, it should be highlighted the ability for *o*-PD-MIP modified electrodes to distinguish 2,4-D and other molecules with small structural differences.

The reliability of *o*-PD-MIP modified electrodes was evaluated by testing the recovery of 2,4-D in suitable spiked real matrices as reported in Table 1. To this end, soil (extracted with pure methanol), river water and tap water samples were spiked with 50 nM 2,4-D. From the recovery values, it was possible to confirm good analytical performance, especially considering the recovery for soil samples (94.4 %), for river water (102.6 %, probably due to the presence of ions complexed within MIP cavities and other organic molecules) and tap water (91.6%), RSD on individual measurement is always ≤9.2 %.

The analytical figures of merits of the proposed *o*-PD-MIP platform were compared to different MIPs reported in literatures for 2,4-D detection (Table 2), showing the lowest limit of detection [21,48–53]. Moreover, the linear range was limited to one order of magnitude due to the different baseline herein considered where *o*-PD-MIPs were incubated with HPLC grade water while usually the template removal curve is considered as baseline.

4. Conclusions

In conclusion, a novel approach for detecting 2,4-D utilizing an *o*-PD-MIP was developed via electropolymerization. The process was monitored *in-situ* using EQCM to analyze both the kinetics, where electrostatic interactions influenced MIP deposition, and the *o*-PD polymer mass, which was found to be comparable for both *o*-PD-MIP and *o*-PD-NIP (approximately 1.7–1.8 μg cm^{-2}). Additionally, the successful removal of the template from the imprinted cavities was confirmed by comparing the XPS spectra of imprinted and *o*-PD-MIPs following various template removal procedures. The most effective method involved a 70:30 mixture of MeOH:H_2O for 15 min under stirring. The developed sensor exhibited excellent sensitivity with a LOD of (3 ± 1) × 10^{-12} M, surpassing the EU regulation limits for drinking water by six orders of magnitude (0.1 mg mL^{-1} or 452.4 μM). Furthermore, the *o*-PD-MIP sensor demonstrated a linear range between 10 and 100pM, displaying exceptional selectivity across the entire tested concentration range (1–1 × 10^6 pM) against structural interferences such as 2,4,5-trichlorophenoxyacetic acid (2,4,5-T, one chloride atom more than 2,4-D) and 2-methyl-4-chlorophenoxyacetic acid (MCPA, one chloride atom replaced by a methyl group), phenoxyacetic acid (PA, aromatic ring without chloride), 4-chlorophenoxyacetic acid (4-CPA, aromatic ring with one chloride atom), 2-(2,4,5-trichlorophenoxy)propionic acid (2-

(2,4,5-T)PA, longer lateral chain) and analytical interferences like parathion. These initial findings underscore the efficacy of the MeOH: H_2O template removal procedure and the straightforward preparation of an *o*-PD-MIP modified gold electrode for the selective detection of 2,4-D in real matrices (recovery: 91.6–102.6 %, with RSD ≤9.2 %) such as soil samples, river and tap water samples.

CRediT authorship contribution statement

Angelo Tricase: Writing – original draft, Investigation, Formal analysis, Data curation. **Verdiana Marchianò:** Investigation, Formal analysis, Data curation. **Eleonora Macchia:** Writing – review & editing, Funding acquisition. **Nicoletta Ditaranto:** Investigation, Formal analysis, Data curation. **Luisa Torsi:** Writing – review & editing, Funding acquisition. **Paolo Bollella:** Writing – review & editing, Writing – original draft, Supervision, Funding acquisition, Conceptualization.

Declaration of competing interest

The authors declare that they have no known competing financial interests or personal relationships that could have appeared to influence the work reported in this paper.

Data availability

Data will be made available on request.

Acknowledgments

The following funding agencies are acknowledged: Centro di Innovazione in Single-Molecule Digital Assay – "Digital Assay" from Regione Puglia DGR N. 218 of 21/02/2022; 1LIVEXYLELLA - ID01 - Trasmissione D. M. n. 664519 del 28/12/2022; NoOne-A binary sensor with single-molecule digit to discriminate biofluids enclosing zero or at least one biomarker, ERC Stg2021, GA:101040383; CSGI is acknowledged for partial financial support.

Supplementary materials

Supplementary material associated with this article can be found, in the online version, at doi:10.1016/j.electacta.2024.144430.

References

[1] M.P. Serbent, A.M. Rebelo, A. Pinheiro, A. Giongo, L.B.B. Tavares, Biological agents for 2,4-dichlorophenoxyacetic acid herbicide degradation, Appl. Microbiol. Biotechnol. 103 (2019) 5065–5078, https://doi.org/10.1007/s00253-019-09838-4.

[2] G. Singh, S. Sharma, A. Singh, A.Devi Mohit, S. Gupta, P. Malik, S. Khurana, S. Soni, Detection of 2,4-dichlorophenoxyacetic acid in water sample by organosilane based silica nanocomposites, Sci. Total Environ. 858 (2023) 159594, https://doi.org/10.1016/j.scitotenv.2022.159594.

[3] K.V. Gobi, H. Tanaka, Y. Shoyama, N. Miura, Highly sensitive regenerable immunosensor for label-free detection of 2,4-dichlorophenoxyacetic acid at ppb levels by using surface plasmon resonance imaging, Sens. Actuators B Chem. 111–112 (2005) 562–571, https://doi.org/10.1016/j.snb.2005.03.118.

[4] P. Bollella, G. Fusco, C. Tortolini, G. Sanzò, R. Antiochia, G. Favero, F. Mazzei, Inhibition-based first-generation electrochemical biosensors: theoretical aspects and application to 2,4-dichlorophenoxy acetic acid detection, Anal. Bioanal. Chem. 408 (2016) 3203–3211, https://doi.org/10.1007/s00216-016-9389-z.

[5] F. Islam, J. Wang, M.A. Farooq, M.S.S. Khan, L. Xu, J. Zhu, M. Zhao, S. Muños, Q. X. Li, W. Zhou, Potential impact of the herbicide 2,4-dichlorophenoxyacetic acid on human and ecosystems, Environ. Int. 111 (2018) 332–351, https://doi.org/10.1016/j.envint.2017.10.020.

[6] R. Girón-Navarro, I. Linares-Hernández, E.A. Teutli-Sequeira, V. Martínez-Miranda, F. Santoyo-Tepole, Evaluation and comparison of advanced oxidation processes for the degradation of 2,4-dichlorophenoxyacetic acid (2,4-D): a review, Environ. Sci. Pollut. Res. 28 (2021) 26325–26358, https://doi.org/10.1007/s11356-021-13730-y.

[7] G. Kaur, B.V.S. Kumar, B. Singh, R.S. Sethi, Exposures to 2,4-dichlorophenoxy-acetic acid with or without endotoxin upregulate small cell lung cancer pathway, J. Occup. Med. Toxicol. 16 (2021) 14, https://doi.org/10.1186/s12995-021-00304-4.

[8] S. Gaaied, M. Oliveira, I. Domingues, M. Banni, 2,4-Dichlorophenoxyacetic acid herbicide effects on zebrafish larvae: development, neurotransmission and behavior as sensitive endpoints, Environ. Sci. Pollut. Res. 27 (2020) 3686–3696, https://doi.org/10.1007/s11356-019-04488-5.

[9] J. Zhou, F. Wang, L. Jia, R. Chai, H. Wang, X. Wang, J. Li, K. Wang, P. Zhang, H. Yang, 2,4-dichlorophenoxyacetic acid induces ROS activation in NLRP3 inflammatory body-induced autophagy disorder in microglia and the protective effect of Lycium barbarum polysaccharide, Environ. Toxicol. 37 (2022) 1136–1151, https://doi.org/10.1002/tox.23471.

[10] E.F.S. Authority, Conclusion on the peer review of the pesticide risk assessment of the active substance 2,4-D, EFSA J. 12 (2014) 3812, https://doi.org/10.2903/j.efsa.2014.3812.

[11] Directive (EU) 2020/2184 of the European parliament and of the council of 16 December 2020 on the quality of water intended for human consumption (recast) (Text with EEA relevance), 2020. http://data.europa.eu/eli/dir/2020/2184/oj/eng (accessed February 9, 2024).

[12] T. Nazim, A. Kubiak, M. Cegłowski, Quantification of 2,4-dichlorophenoxyacetic acid in environmental samples using imprinted polyethyleneimine with enhanced selectivity as a selective adsorbent in ambient plasma mass spectrometry, J. Hazard. Mater. (2024) 133661, https://doi.org/10.1016/j.jhazmat.2024.133661.

[13] M. Mohammadnia, R. Heydari, M.R. Sohrabi, Determination of 2,4-Dichlorophenoxyacetic acid in food and water samples using a modified graphene oxide sorbent and high-performance liquid chromatography, J. Environ. Sci. Health Part B (55) (2020) 293–300, https://doi.org/10.1080/03601234.2019.1692613.

[14] S. Moret, M. Hidalgo, J.M. Sanchez, Hollow-Fiber Liquid-Phase Microextraction (HF-LPME) Coupled On-Line to Liquid Chromatography for the Determination of the Herbicides 2,4-Dichlorophenoxyacetic Acid and 2-Methyl-4-chlorophenoxy-acetic Acid and Their Main Metabolites in Soil Samples, Separations. 10 (2023) 273, https://doi.org/10.3390/separations10050273.

[15] N. Orooji, A. Takdastan, R.J. Yengejeh, S. Jorfi, A.H. Davami, A quick and inexpensive method to determine 2, 4-dichlorophenoxyacetic acid residues in water samples by HPLC, Desalin. Water Treat. 217 (2021) 329–338.

[16] M. Kodali, S. Herrera, S. Kabir, A. Serov, C. Santoro, I. Ieropoulos, P. Atanassov, Enhancement of microbial fuel cell performance by introducing a nano-composite cathode catalyst, Electrochim. Acta 265 (2018) 56–64.

[17] A. Gubin, P. Sukhanov, A. Kushnir, K. Shikhaliev, M. Potapov, E. Kovaleva, Ionic-liquid-modified magnetite nanoparticles for MSPE-GC–MS determination of 2,4-D butyl ester and its metabolites in water, soil, and bottom sediments, Environ. Nanotechnol. Monit. Manag. 17 (2022) 100652, https://doi.org/10.1016/j.enmm.2022.100652.

[18] Y. Chen, X. Wu, Y. Li, Y. Yang, D. Yang, S. Yin, L. Liu, C. Sun, Simultaneous determination of seven plant growth regulators in melons and fruits by modified QuEChERS coupled with capillary electrophoresis, Food Anal. Methods 11 (2018) 2788–2798, https://doi.org/10.1007/s12161-018-1266-2.

[19] I. Silvestro, M. Fernández-García, C. Ciarlantini, I. Francolini, A. Girelli, A. Piozzi, Molecularly imprinted polymers based on chitosan for 2,4-dichlorophenoxyacetic acid removal, Int. J. Mol. Sci. 23 (2022) 13192, https://doi.org/10.3390/ijms232113192.

[20] F. Azadmehr, K. Zarei, An imprinted polymeric matrix containing DNA for electrochemical sensing of 2,4–dichlorophenoxyacetic acid, Microchim. Acta 186 (2019) 814, https://doi.org/10.1007/s00604-019-3980-x.

[21] O. Cakir, M. Bakhshpour, F. Yilmaz, Z. Baysal, Novel QCM and SPR sensors based on molecular imprinting for highly sensitive and selective detection of 2,4-dichlorophenoxyacetic acid in apple samples, Mater. Sci. Eng. C 102 (2019) 483–491, https://doi.org/10.1016/j.msec.2019.04.056.

[22] Z.F. Li, J.X. Dong, N. Vasylieva, Y.L. Cui, D.B. Wan, X.D. Hua, J.Q. Huo, D.C. Yang, S.J. Gee, B.D. Hammock, Highly specific nanobody against herbicide 2,4-dichlorophenoxyacetic acid for monitoring of its contamination in environmental water, Sci. Total Environ. 753 (2021) 141950, https://doi.org/10.1016/j.scitotenv.2020.141950.

[23] G. Fusco, F. Gallo, C. Tortolini, P. Bollella, F. Ietto, A. De Mico, A. D'Annibale, R. Antiochia, G. Favero, F. Mazzei, AuNPs-functionalized PANABA-MWCNTs nanocomposite-based impedimetric immunosensor for 2,4-dichlorophenoxy acetic acid detection, Biosens. Bioelectron. 93 (2017) 52–56, https://doi.org/10.1016/j.bios.2016.10.016.

[24] F. Di Nardo, L. Anfossi, C. Baggiani, MIP-based immunoassays: a critical review, Anal. Chim. Acta 1277 (2023) 341547, https://doi.org/10.1016/j.aca.2023.341547.

[25] G. Selvolini, G. Marrazza, MIP-based sensors: promising new tools for cancer biomarker determination, Sensors 17 (2017) 718.

[26] A. Speltini, A. Scalabrini, F. Maraschi, M. Sturini, A. Profumo, Newest applications of molecularly imprinted polymers for extraction of contaminants from environmental and food matrices: a review, Anal. Chim. Acta 974 (2017) 1–26, https://doi.org/10.1016/j.aca.2017.04.042.

[27] F. Parnianchi, S. Kashanian, M. Nazari, C. Santoro, P. Bollella, K. Varmira, Highly selective and sensitive molecularly imprinting electrochemical sensing platform for bilirubin detection in saliva, Microchem. J. 168 (2021) 106367.

[28] S. Cavalera, M. Chiarello, F. Di Nardo, L. Anfossi, C. Baggiani, Effect of experimental conditions on the binding abilities of ciprofloxacin-imprinted nanoparticles prepared by solid-phase synthesis, React. Funct. Polym. 163 (2021) 104893, https://doi.org/10.1016/j.reactfunctpolym.2021.104893.

[29] C.C. Villa, L.T. Sánchez, G.A. Valencia, S. Ahmed, T.J. Gutiérrez, Molecularly imprinted polymers for food applications: a review, Trends Food Sci. Technol. 111 (2021) 642–669, https://doi.org/10.1016/j.tifs.2021.03.003.
[30] S. Bhakta, P. Mishra, Molecularly imprinted polymer-based sensors for cancer biomarker detection, Sens. Actuators. Rep. 3 (2021) 100061.
[31] J. Wackerlig, R. Schirhagl, Applications of molecularly imprinted polymer nanoparticles and their advances toward industrial use: a review, Anal. Chem. 88 (2016) 250–261, https://doi.org/10.1021/acs.analchem.5b03804.
[32] E. Mazzotta, S. Rella, A. Turco, C. Malitesta, Electrosynthesized molecularly imprinted polymers for chemosensing: fundamentals and applications, Ch. 13, in: W. Kutner, P.S. Sharma (Eds.), Molecularly Imprinted Polymers for Analytical Chemistry Applications, Royal Society of Chemistry, London, 2018, p. 412.
[33] C. Yan, R. Zhang, Y. Chen, G. Wang, Electrochemical determination of enrofloxacin based on molecularly imprinted polymer via one-step electro-copolymerization of pyrrole and o-phenylenediamine, J. Electroanal. Chem. 806 (2017) 130–135, https://doi.org/10.1016/j.jelechem.2017.10.047.
[34] A. Yarman, S. Kurbanoglu, I. Zebger, F.W. Scheller, Simple and robust: the claims of protein sensing by molecularly imprinted polymers, Sens. Actuators B Chem. 330 (2021) 129369.
[35] A. Yarman, S. Kurbanoglu, K.J. Jetzschmann, S.A. Ozkan, U. Wollenberger, F. W. Scheller, Electrochemical MIP-sensors for drugs, Curr. Med. Chem. 25 (2018) 4007–4019, https://doi.org/10.2174/0929867324666171005103712.
[36] A. Ellwanger, C. Berggren, S. Bayoudh, C. Crecenzi, L. Karlsson, P.K. Owens, K. Ensing, P. Cormack, D. Sherrington, B. Sellergren, Evaluation of methods aimed at complete removal of template from molecularly imprinted polymers, Analyst 126 (2001) 784–792.
[37] R.A. Lorenzo, A.M. Carro, C. Alvarez-Lorenzo, A. Concheiro, To remove or not to remove? The challenge of extracting the template to make the cavities available in molecularly imprinted polymers (MIPs), Int. J. Mol. Sci. 12 (2011) 4327–4347.
[38] B.S. Batlokwa, J. Mokgadi, T. Nyokong, N. Torto, Optimal template removal from molecularly imprinted polymers by pressurized hot water extraction, Chromatographia 73 (2011) 589–593.
[39] E. Mazzotta, S. Rella, A. Turco, C. Malitesta, XPS in development of chemical sensors, RSC Adv. 5 (2015) 83164–83186.
[40] E. Mazzotta, T. Di Giulio, C. Malitesta, Electrochemical sensing of macromolecules based on molecularly imprinted polymers: challenges, successful strategies, and opportunities, Anal. Bioanal. Chem. (2022) 1–36.
[41] J.F. Watts, J. Wolstenholme, An Introduction to Surface Analysis By XPS and AES, John Wiley & Sons, 2019. https://books.google.com/books?hl=en&lr=&id=kDy5DwAAQBAJ&oi=fnd&pg=PP11&dq=Watts,+John+F.,+and+John+Wolstenholme.+An+introduction+to+surface+analysis+by+XPS+and+AES.+John+Wiley+%26+Sons,+2019&ots=IQ-DAy3ibE&sig=3cMRBCIT3AgeLPRNx-0roRL8KLI (accessed October 13, 2023).
[42] I. Losito, F. Palmisano, P.G. Zambonin, o-Phenylenediamine electropolymerization by cyclic voltammetry combined with electrospray ionization-ion trap mass spectrometry, Anal. Chem. 75 (2003) 4988–4995, https://doi.org/10.1021/ac0342424.
[43] D.H. Garabrant, M.A. Philbert, Review of 2,4-Dichlorophenoxyacetic Acid (2,4-D) epidemiology and toxicology, Crit. Rev. Toxicol. 32 (2002) 233–257, https://doi.org/10.1080/20024091064237.
[44] J. Kankare, Sauerbrey Equation of Quartz Crystal Microbalance in Liquid Medium, Langmuir 18 (2002) 7092–7094, https://doi.org/10.1021/la025911w.
[45] M. Valentino, A. Imbriano, A. Tricase, F. Della Pelle, D. Compagnone, E. Macchia, L. Torsi, P. Bollella, N. Ditaranto, Electropolymerized molecularly imprinted polypyrrole film for dimethoate sensing: investigation on template removal after the imprinting process, Anal. Methods 15 (2023) 1250–1253, https://doi.org/10.1039/D2AY02024F.
[46] S. Liu, B. Yu, T. Zhang, Preparation of crumpled reduced graphene oxide–poly (p-phenylenediamine) hybrids for the detection of dopamine, J. Mater. Chem. A 1 (2013) 13314–13320.
[47] J. Chastain, R.C. King Jr, Handbook of X-ray photoelectron spectroscopy, Perkin Elmer Corporation 40 (1992) 221.
[48] F. Omidi, M. Behbahani, S. Samadi, A. Sedighi, S.J. Shahtaheri, Coupling of molecular imprinted polymer nanoparticles by high performance liquid chromatography as an efficient technique for sensitive and selective trace determination of 4-chloro-2-methylphenoxy acetic acid in complex matrices, Iran. J. Public Health 43 (2014) 645–657.
[49] N.Y. Limaee, S. Rouhani, M.E. Olya, F. Najafi, Selective 2,4-dichlorophenoxyacetic acid optosensor employing a polyethersulfone nanofiber-coated fluorescent molecularly imprinted polymer, Polymer 177 (2019) 73–83, https://doi.org/10.1016/j.polymer.2019.05.067. . (Guildf).
[50] G. Guan, S. Wang, H. Zhou, K. Zhang, R. Liu, Q. Mei, S. Wang, Z. Zhang, Molecularly imprinted polypyrrole nanonecklaces for detection of herbicide through molecular recognition-amplifying current response, Anal. Chim. Acta 702 (2011) 239–246.
[51] A.K. Prusty, S. Bhand, A capacitive sensor for 2, 4-D determination in water based on 2, 4-D imprinted polypyrrole coated pencil electrode, Mater. Res. Express. 4 (2017) 035306.
[52] T.S. Anirudhan, S.M. Anju, Synthesis and evaluation of TiO2 nanotubes/silylated graphene oxide-based molecularly imprinted polymer for the selective adsorption and subsequent photocatalytic degradation of 2, 4-Dichlorophenoxyacetic acid, J. Environ. Chem. Eng. 7 (2019) 103355.
[53] Y. Liu, Y. He, Y. Jin, Y. Huang, G. Liu, R. Zhao, Preparation of monodispersed macroporous core–shell molecularly imprinted particles and their application in the determination of 2,4-dichlorophenoxyacetic acid, J. Chromatogr. A 1323 (2014) 11–17, https://doi.org/10.1016/j.chroma.2013.11.002.